Article

Journal of
Nanoscience and Nanotechnology
Vol. 17, 3959–3966, 2017
www.aspbs.com/jnn

Nitrogen-Doped Graphene Supported Cobalt Oxide Nanocomposite as High Performance Electrocatalyst for Oxygen Reduction Reaction

Sabina Yasmin, Mohammad Shamsuddin Ahmed, and Seungwon Jeon*

Department of Chemistry and Institute of Basic Science, Chonnam National University, Gwangju 500-757, Republic of Korea

Nitrogen doped reduced graphene oxide-supported cobalt oxide catalyst has been synthesized by a simple one step chemical reduction method (denoted as NrGO–Co_3O_4) for electrocatalytic oxygen reduction reaction (ORR). This material has been characterized by various instrumental methods. The morphological analysis shows the Co_3O_4 nanocomposites are well set on to the reduced graphene oxide with better dispersion. The X-ray photoelectron spectroscopy (XPS) shows electrochemical reduction has been done successfully with the increasing C/O ratio. Also, the Raman data reveals that the Co is presents with the oxidized form. The electrocatalytic activities have been verified using cyclic voltammetry (CV) and hydrodynamic voltammetry techniques in 0.1 M KOH electrolyte. The as prepared catalyst has shown more positively shifted onset and half wave potential (−0.091 V and −0.276 vs. Ag/AgCl) and high cathodic current density 2.57 mA cm^{-2} and high methanol, ethanol crossover tolerance than Pt/C. It is the introduction of strongly bonded cobalt nanocomposite into the network of NrGO that modulate the electronic properties of the NrGO–Co_3O_4, resulting in the superb electrocatalytic performance. The reaction kinetics have confirmed that the ORR at NrGO–Co_3O_4 catalyst follows a four electron transfer reaction process.

Keywords: Cobalt Oxide, Fuel Cell, Nanocomposites, Nitrogen Doping, Oxygen Reduction Reaction, Reduced Graphene Oxide.

1. INTRODUCTION

Catalysts for the oxygen reduction reaction (ORR) are the key components of fuel cells (FCs).[1] Platinum (Pt)-based catalysts are commonly utilized as the best electrocatalysts for both anode and cathode in FCs due to the excellent catalytic activity. Although, the large-scale commercialization of FCs is impeded by the high cost and limited reserves of Pt.[2, 3] In order to reduce the usage of precious Pt metal and subsequently the cost of (FCs), the development of nonprecious metal or metal-free ORR electrocatalysts has generated a great deal of interest.[4–9] Metal or metal oxide catalysts frequently suffer from dissolution, sintering, and agglomeration during catalysis, which can result in catalyst degradation.[10] To overcome this obstacle, nano-based support materials such as carbon (active carbon, porous carbon, carbon nanotubes, and/or graphene) have been introduced to nanocatalysts for maximizing electroactive surface area and improve their catalytic activity including durability.[10]

It is, however, among all kinds of FCs, alkaline fuel cells (AFCs) are the most attractive due to their superior kinetic activity for the ORR than that of FCs which utilizing acidic media. In addition, AFCs do not require precious metals for stable activity.[11] The ORR takes place in the cathode electrode and could be followed by two main pathways as below:

$$O_2 + 4e^- + 4H^+ \longrightarrow 4H_2O \quad (1)$$

$$O_2 + 2e^- + 2H^+ \longrightarrow H_2O_2 + 2e^- + 2H^+ \longrightarrow 2H_2O \quad (2)$$

In Eq. (1), O_2 undergoes a single-step four-electron transferred reduction, directly forming H_2O; meanwhile, in Eq. (2), O_2 first undergoes a two-electron reduction to H_2O_2, followed by an additional two-electron reduction to H_2O.[12] Therefore, because H_2O_2 production inhibits the efficiency of FC, the development of a system that favors the four-electron reduction pathway is crucially needed.

Graphene sheets are highly conductive and 2D flat lattices consisting of a monolayer of sp^2-hybridized carbon atoms which have been attracted a great deal of research

*Author to whom correspondence should be addressed.

interest due to high electrical conductivity and electron mobility, large surface area, long-term stability and unique mechanical flexibility.[13–15] Graphene has already been used in various fields, especially in sensors,[16, 17] capacitor[18, 19] and ORR catalysts.[4–6]

N-doped reduced graphene oxide (NrGO) has been reported to be good catalyst as well as good support for ORR because of its large surface area, high electric conductivity, and N-related active sites.[20, 21] Therefore, cobalt nanocomposite directly grown on the surface of N-doped graphene support would be superior catalyst with improved catalytic performance for ORR.

In this article, we demonstrate N-doped reduced graphene oxide supported cobalt oxide (NrGO–Co_3O_4) which synthesized by simple chemical reaction. Co_3O_4 has been extensively studied due to high capacities and multi-electron reaction ability in the electrochemical reaction.[22] Meanwhile, Graphene-based metal oxide or their alloy composites have shown superior electrocatalytic properties.[16, 23–25] Reduced-graphene is recognized as a potential conductive support material to improve the electrochemical properties of Co-based materials.[22] The as prepared NrGO–Co_3O_4 was characterized via X-ray photoelectron spectroscopic (XPS), Transmission electron microscopy (TEM) and Raman spectroscopy. The electrochemical behavior of NrGO–Co_3O_4 for ORR has been investigated using cyclic voltammetry (CV), rotating disk electrode (RDE) and rotating ring disk electrode (RRDE) techniques in 0.1 M KOH solutions. In the electrochemical study, we found that the NrGO–Co_3O_4 exhibits a more positive onset potential (E_{onset}), higher cathodic current density, lower H_2O_2 yield, and higher electron transfer kinetics for the ORR in alkaline media. The results prove that the NrGO–Co_3O_4 fabricated glassy carbon electrode (GCE) has superior electrocatalytic activity for ORR than that of NrGO and Pt/C.

2. EXPERIMENTAL DETAILS

2.1. Instruments

The field emission transmission electron microscopy (FE-TEM) and energy-dispersive X-ray spectroscopy (EDX) observations were carried out in a JEM-2100F microscope at 200 kV. The X-ray photoelectron spectroscopy (XPS) measurements were performed on a Multi Lab 2000 (Thermo Electron Corporation, England) with a 14.9 keV Al Ka X-ray source. A three-electrode potentiostat (CHI 700C Electrochemical Workstation, USA) in a grounded Faraday cage was used for voltammetric measurements. A Pt wire was used as an auxiliary electrode. A calibrated Ag/AgCl electrode from Bioanalytical Systems Inc. (BAS) in 3 M NaCl solution was used as a reference electrode. The current densities were normalized with respect to the geometrical surface area of electrodes. An RRDE was employed as a working electrode. An EG&G Model 636 RRDE system and a CHI 700C electrochemical workstation were used for hydrodynamic voltammetry.

2.2. Materials and Chemicals

Graphite powder (~325 mesh, 99.999%), hydrazine monohydrate (65%) were from Aldrich, Korea. Cobalt(II) nitrate hexahydrate [$Co(NO_3)_2 \cdot 6H_2O$] was purchased from Daejung Co., Korea. All other reagents were of analytical grade and used without further purification.

2.3. Preparation of NrGO–Co_3O_4 Nanocomposite

GO was synthesized by using the modified Hummer's method[3, 26] through oxidation of graphite powder. The NrGO–Co_3O_4 synthesis procedure has shown in Scheme 1. In this procedure, GO (in 10 mg mL^{-1} in water) was taken into a 25 mL bottle and sonicated for 1 h for making homogeneous GO suspension. 8 mL of 10 mM $Co(NO_3)_2 \cdot 6H_2O$ solution was then added drop wise into GO suspension with magnetic stirring and then sonication further for 30 minutes. Then 10 μL of N_2H_4 (65%) added under continuous stirring then heating at 65 °C for overnight night. Then, the product was cooled, filtered and washed several times with DI water. Finally the product was dried at 45 °C under vacuum condition for 24 h. For comparison, NrGO was prepared through same way without addition of $Co(NO_3)_2$.

2.4. Fabrication of NrGO–Co_3O_4 Modified GCE

The surfaces of GCE (diameter: 3 mm) or rotating ring disk electrode (RRDE, GC disk area: 0.196 cm^2) were carefully polished with 0.05 μm alumina pastes, washed several times with distilled water and rinse with methanol to remove the physically adsorbed particles. The suspension of NrGO–Co_3O_4 in ethanol (1 mg mL^{-1}) was

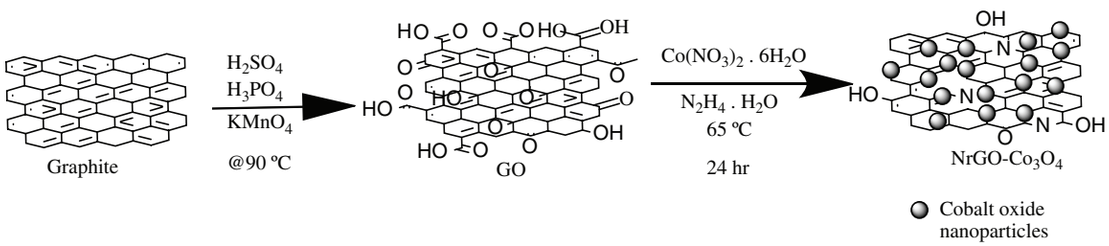

Scheme 1. Synthesis procedure of NrGO–Co_3O_4 preparation.

prepared by 1 h ultrasonic agitation. Exactly 10 μL of NrGO–Co_3O_4 suspension was then drop coated onto the polished GCE (16 μL for RRDE) and the allowed to dry in air. All electrochemical experiments were performed in a high purity oxygen or Argon purged (for at least 30 min) 0.1 M KOH solution at room temperature (~26 °C).

3. RESULTS AND DISCUSSION

3.1. Instrumental Characterizations

The surface morphology of NrGO and NrGO–Co_3O_4 has investigated via TEM analysis. The TEM images of simply prepared NrGO and NrGO–Co_3O_4 are shown in Figure 1. The TEM image of NrGO exhibits a silky waves-like morphology (Fig. 1(a)). It shows a transparent sheet-like structure and turned it blackish when it's layered, indicating a broadened surface area. The TEM images of NrGO–Co_3O_4 reveal that the as-formed Co_3O_4 (NPs) were homogeneously and uniformly disperse onto the surface of the NrGO demonstrating Co_3O_4NPs were set successfully onto the NrGO without excess aggregation (Fig. 1(b)). The EDX spectrum of NrGO–Co_3O_4 (Fig. 1(c)) shows signals from C, O, Co and Cu (Cu peak was attributable to the TEM holder). Indicating the NrGO–Co_3O_4 contained only cobalt oxide with good population and without any considerable metal contamination.

The XPS spectra were performed to investigate the composition of the samples. Figure 2 shows the XPS survey spectra of NrGO and NrGO–Co_3O_4 samples. The survey spectra exhibit that three different peaks at about 285 eV, 533 eV, and 400 eV which corresponding to the C1*s*, O1*s* and, N1*s* respectively.[27–31] Only Co indicated peak was observed along with all above mentioned peaks in NrGO–Co_3O_4 upon Co addition (Fig. 2(a)). Figure 2(b) shows the high-resolution C1*s* spectra of NrGO and NrGO–Co_3O_4. The binding energies of 285.0 eV, 286.6 eV, 287.7 eV and 289.9 eV were attributed to the C–C/C═C, C–O, C═O and O–C═O bonds, respectively.[28] The intensity of oxygenated groups, especially for C–O and C═O, significantly decreased compared to C–C/C═C bond, confirming that GO was successfully reduced by reducing agent for both NrGO and NrGO–Co_3O_4 samples. In Figure 2(c), high resolution spectra N1*s* at binding energy of 400 eV of NrGO and NrGO–Co_3O_4 indicate N doping was successful. The relatively high intensity of the N peak corresponds to a high content (5.22 at%) for NrGO and (5.29 at%) for NrGO–Co_3O_4. The corresponding peak of N1*s* spectrum of NrGO and NrGO–Co_3O_4 indicate the pyridinic N (N1, 399.7 eV) and graphitic N (N2, 401.5 eV) and oxygenated N (N3, 405.6 eV).[26, 32]

A Co2*p* spectrum of NrGO–Co_3O_4 is presenting in Figure 2(d). As shown in Figure 2(d), the Co2*p* spectrum contains of two segments of peaks leveled as Co2$p_{3/2}$ and Co2$p_{1/2}$, respectively.[33, 34] The presence of the Co2$p_{3/2}$ and Co2$p_{1/2}$ peaks are fitted considering two spin–orbit doublets characteristic of Co^{2+} and Co^{3+}, respectively, in almost equal ration.[33]

Raman spectroscopy can be used to characterize the structural and electronic properties of carbon materials. Figure 3 displays the Raman spectra of NrGO and NrGO–Co_3O_4 which consists of a set of distinct peaks. The peaks at 1354 cm^{-1} and 1596 cm^{-1} can be ascribed to the D and G bands, respectively. The characteristic G band is associated with the sp^2 carbon atom vibrations and the D peak is due to the breathing modes of six-atom rings and requires a defect for its activation.[30, 31, 35] The ratios of the intensities of D band to G band (I_D/I_G) was used to understand the structural disorder which was slightly decreased from 1.28 to 1.18 for NrGO to NrGO–Co_3O_4, respectively, because of the decrease in the sp^2 domain size of carbon atoms and the reduction of sp^3 to sp^2 carbon during the chemical reaction.[36] The G band of NrGO–Co_3O_4 is negatively shifted than that of NrGO, due to the $\pi-\pi$ interaction between Co_3O_4NPs and graphene (Fig. 3 inset)[31] which signifying well attachment of NPs onto graphene sheet and better structural features.[36]

3.2. ORR on Modified Electrodes

3.2.1. CV Study

The electrocatalytic activity of NrGO–Co_3O_4 for ORR was initially examined by CV in the potential range from 0.2 to −1.0 V versus Ag/AgCl at a scan rate of 50 mV s^{-1}. As shown in Figures 4(a, b) in the Ar-saturated 0.1 M KOH

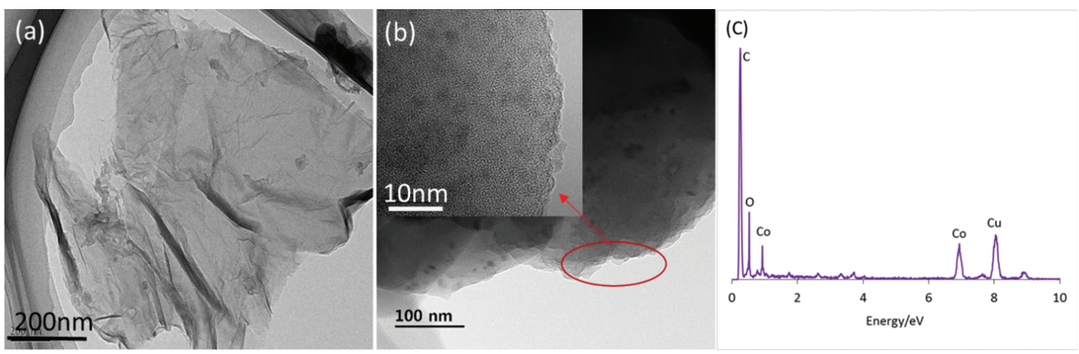

Figure 1. TEM images of NrGO (a), NrGO–Co_3O_4 (b), and EDX spectrum of NrGO–Co_3O_4 (c); inset: the HRTEM image of NrGO–Co_3O_4.

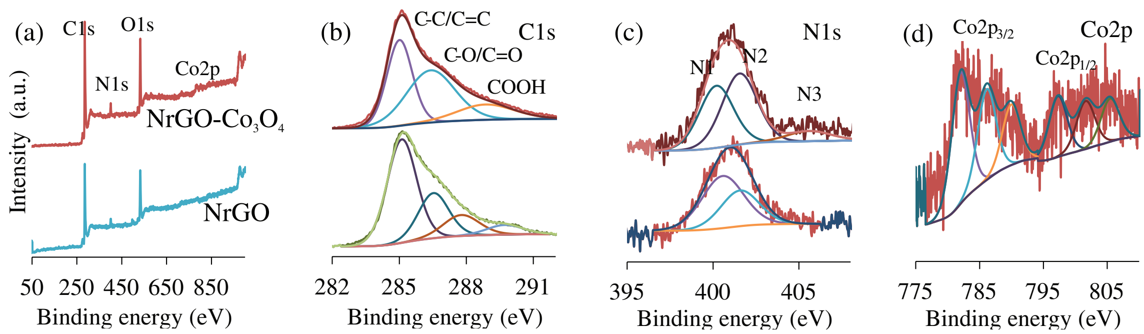

Figure 2. XPS survey spectra (a), core level of C1*s* (b) and N1*s* (c) of NrGO and NrGO–Co_3O_4 and Co2*p* spetram of NrGO–Co_3O_4 (d).

solution, a featureless voltammogram without any evident peak is observed. In contrast, as the KOH solution is saturated with O_2, a well-defined and strong cathodic peak occurs, indicating the high catalytic activities of NrGO–Co_3O_4 for ORR. The E_{onset} shifted positively to around −0.112 V with increasing peak current density (2.57 mA cm^{-1}) than NrGO (E_{onset} − 0.2, current density 0.81 mA cm^{-1}). This result clearly indicates that the ORR catalytic activity of NrGO–Co_3O_4 is greater than that of NrGO due to incorporation of Co_3O_4NPs onto NrGO which acting as more active site for ORR.

We further evaluated the catalytic activity of NrGO, NrGO–Co_3O_4 and commercial 20% Pt/C catalysts toward ORR by the rotating disk electrode (RDE) measurements which recorded at a constant rotation speed of 1600 rpm in an O_2-saturated 0.1 M KOH solution at 10 mV s^{-1} scan rate. As shown in Figure 5, the linear sweep voltammetry (LSV) curves on RDE confirm the superior catalytic activity of NrGO–Co_3O_4 with the E_{onset} of −0.091 V, whereas the E_{onset} of ORR NrGO is −0.187 V. In addition, the ORR current density at any potential and half-wave potential ($E_{1/2}$) for NrGO–Co_3O_4 both are higher than that of NrGO. Although, the ORR E_{onset} and $E_{1/2}$ for NrGO–Co_3O_4 are lower than that of a commercial Pt/C electrode, but the limiting current density (J_L, from −0.8 V) is higher than that of Pt/C. It is, however, the ease with which conventional graphene materials can be converted into cost-effective ORR electrocatalysts simply by the addition of nonprecious metal oxide and simple chemical treatment suggest considerable room for cost-effective preparation of various nonprecious metal oxide catalysts for ORR. These experimental results suggest that the catalytic activity of ORR at NrGO–Co_3O_4 is obviously better than that of NrGO catalyst in respect to any parameters (E_{onset}, $E_{1/2}$, or J_L) and more or less good than Pt/C in respect to the J_L. It is undoubted that the well-dispersion Co_3O_4 NPs and better reduction degree of NrGO play the key role for ORR activity enhancement of this catalyst.

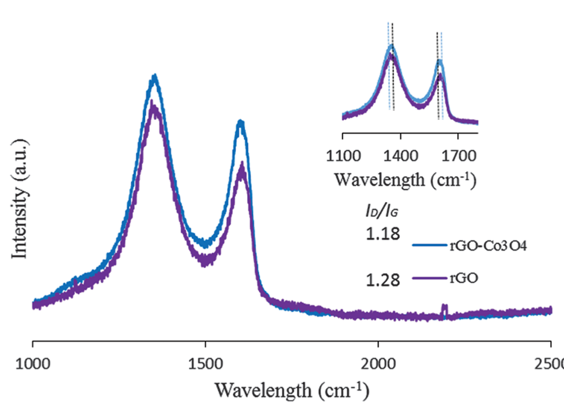

Figure 3. Raman spectra of NrGO and NrGO–Co_3O_4; inset: G and D bands.

3.2.2. Hydrodynamic Voltammetry Study

The RDE hydrodynamic voltammetry is widely used for the determination of the electrocatalytic ORR pathway. The electrocatalytic activity of ORR was then evaluated by hydrodynamic voltammetry measurements in an O_2-saturated 0.1 M KOH solution in Figure 6. Figure 6 shows the RDE voltammograms of the glassy carbon disk electrode modified with NrGO (a) NrGO–Co_3O_4 (b) with the electrode rotation rate varied from 100 to 3600 rpm at scan rate of 10 mV s^{-1}. The increase in current with faster rotating rates is actually expected, as faster rotating rates correlate with faster O_2 flux to the catalyst surface. The ORR J_L of the NrGO–Co_3O_4 modified electrode was always larger than that of the NrGO electrode at any constant rotation rate. The Koutecky–Levich (K–L) plots which are plotted from the plateau current show linear dependence at cited potentials (5a′–b′). The linearity and the parallelism of K–L plots are usually represented first order kinetics with respect to O_2 [30] and the similar transferred electron number for per O_2.[35]

Therefore, the transferred electron number (n) per O_2 involved in ORR was calculated from the K–L equation as given below.[37]

$$J^{-1} = J_K^{-1} + J_L^{-1} \quad (3)$$

$$J_L = 0.62nFAC_o(D_o)^{2/3}V^{-1/6}\omega^{1/2} \quad (4)$$

where J and J_K are the measured and kinetic current density, ω is the rotating rate (rpm), F is the Faraday constant (96,485 C mol^{-1}), C_o is the concentration of O_2

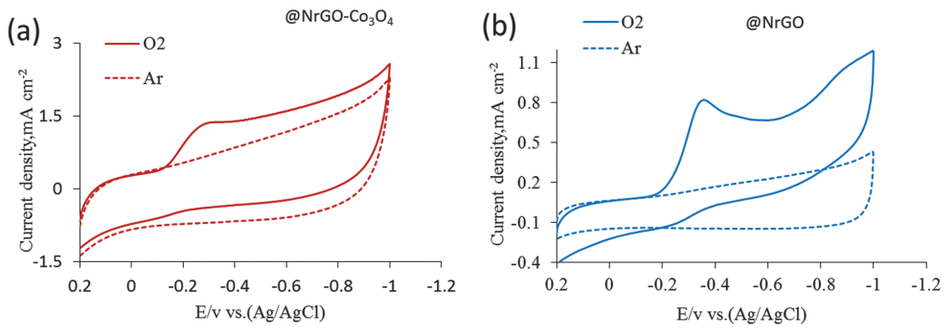

Figure 4. The CVs for ORR on NrGO–Co_3O_4 (a), NrGO (b) at 50 mV s^{-1} scan rate in O_2 (solid line) and Ar (dotted line) saturated 0.1 M KOH.

in the electrolyte (1.2 mmol L^{-1}),[3, 37, 38] D_o is the diffusion coefficient of O_2 in the 0.1 M KOH solution (1×10^{-5} cm^2 s^{-1}),[3, 38] and ν is the kinetic viscosity of the electrolyte (1×10^{-2} cm^2 s^{-1}).[34, 35, 39]

3.2.3. Kinetic Analysis

To further investigate the electron transfer pathway, the RRDE voltammograms of the NrGO, NGO–Co_3O_4 and Pt/C have been carried out in the same electrolyte solution with the electrode rotation rate 1600 rpm at scan rate of 10 mV s^{-1} in Figure 7. Figure 7(a) shows better J_L on NrGO–Co_3O_4 even than that of commercially available Pt/C at disk electrode. The ring current is actually corresponded to the amount of hydrogen peroxide (H_2O_2) which generated at the disk electrode during ORR. Very importantly, the corresponding ring electrode current density was much lower at NrGO–Co_3O_4 than NrGO suggesting a minimal amount of H_2O_2 intermediate was produced at NrGO–Co_3O_4 during ORR and hence high efficiency of the electrocatalytic ORR process.

Another calculation method had been used to verify the n value using ring and disk electrodes current density of RRDE measurement. However, the n value and the percentage (%) of produced H_2O_2 at modifier electrodes during O_2 reduction were calculated from the equations as below:[40, 41]

$$n = \frac{4i_d}{id + (i_r/N)} \tag{5}$$

$$\%\ \text{of}\ H_2O_2 = \frac{200i_r/N}{i_d + i_r/N} \tag{6}$$

where, i_d is the current of disk electrode, i_r is the current of ring electrode and $N = 0.18$, which is the RRDE collection efficiency. The n value and the % of H_2O_2 calculated using Eqs. (5) and (6) using obtained current data from Figure 7(a). According to Figure 7(b), the transferred electron at NrGO–Co_3O_4 and Pt/C was closer to the four and was always higher than NrGO. Also, the corresponding % of H_2O_2 at NrGO–Co_3O_4 and Pt/C was lower than that of NrGO (in Fig. 7(c)) suggesting that a significant amount (80%) of O_2 is reduced directly to H_2O at this NrGO–Co_3O_4 modified electrode compared with other tested catalysts.

Finally, the mass transport corrected Tafel plots were produced to further investigate the kinetic properties for the NrGO, NrGO–Co_3O_4 and Pt/C electrodes (Fig. 7(d)).

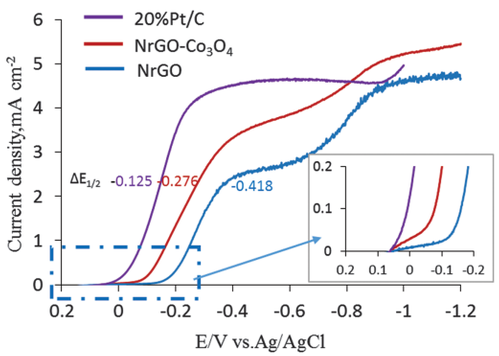

Figure 5. LSV curves of the NrGO, NrGO–Co_3O_4 and Pt/C electrocatalyst in O_2-saturated 0.1 M KOH solution at a scan rate of 10 mV s^{-1} and at rotation speed of 1600 rpm.

Table I. The summary of the ORR performance on NrGO, NrGO–Co_3O_4 and 20% Pt/C electrodes.

Name	NrGO	NrGO–Co_3O_4	20% Pt/C
E_{onset} from LSV (V)	−0.187	−0.091	0.042
$E_{1/2}$ (V)	−0.418	−0.276	−0.125
j_k (mA cm^{-2}) @ −0.9 V	4.37	4.98	4.98
% of H_2O_2 at −1.0 V	20.1	15.4	15.7
Tafel slope (mV dec^{-1})	131	120	119
n value @ −1.0 V	3.6	3.9	4

Table II. Comparison of different cobalt oxide-based catalysts for ORR.

Name	E_{onset} (V)	$E_{1/2}$ (V)	j_k @ −0.8 V (mA cm^{-2})	n value	Refs.
NrGO–Co_3O_4	−0.091	−0.276	4.98	3.9	This work
Co-NGA	−0.16		4.80	–	[47]
MnO_x–Co_3O_4/C	−0.056	−0.116	~2.3	3.9	[48]
Co_3O_4	−0.233		2.1	2	[49]
CMO/GA	−0.10	−0.22		4.00	[50]

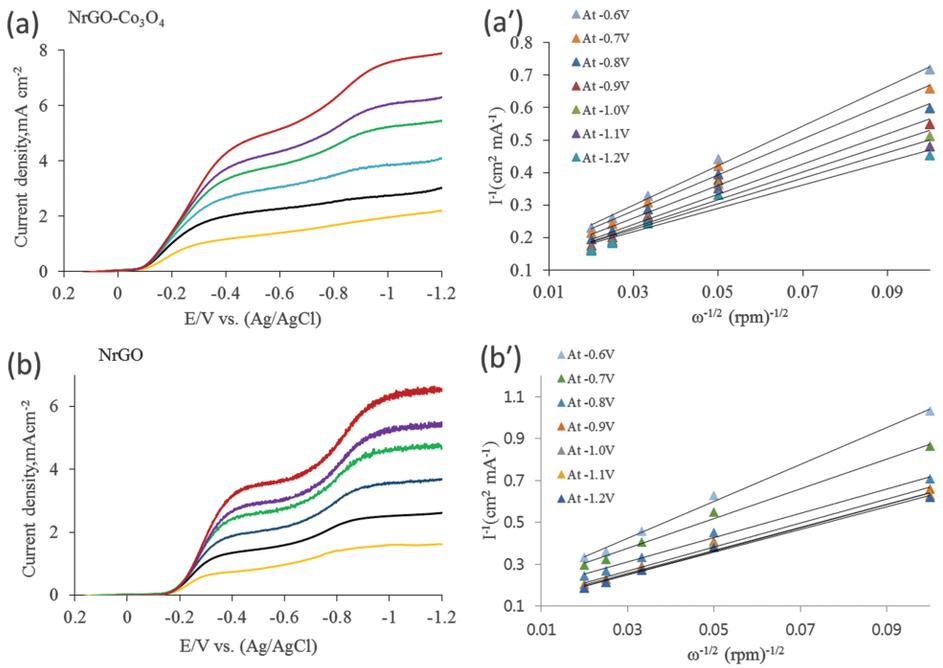

Figure 6. RDE voltammograms for ORR on NrGO–Co_3O_4 (a), and NrGO (b) at various rpm in O_2-saturated 0.1 M KOH at scan rate of 10 mV s^{-1}; and their corresponding K–L plots (a′) and (b′).

Two Tafel slopes are commonly seen in a Tafel plot such as, 120 mV dec^{-1} and 60 mV dec^{-1}. The 120 mV dec^{-1} indicates the first electron transfer is the rate determining step to the transport of O_2 to the electrocatalyst.[42, 43] The Tafel slopes were obtained at high overpotential where the reaction speed is dominated by the diffusion limitation inside the material. The Tafel slope of the NrGO–Co_3O_4 has yielded the lower value of 120.5 mV dec^{-1} than that of NrGO (131 mV dec^{-1}), and closely followed by the Pt/C (118 mV dec^{-1}), revealing the apparently facilitated mass

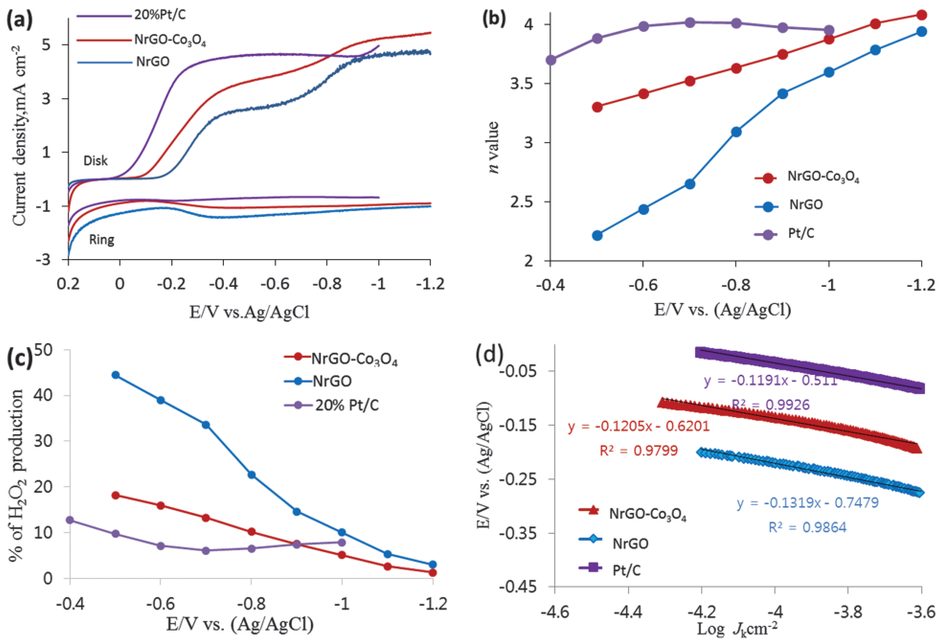

Figure 7. RRDE voltammograms at NrGO, NrGO–Co_3O_4 and Pt/C modified electrodes at 1600 rpm and at 10 mV s^{-1} scan rate in O_2-saturated 0.1 M KOH (a), the corresponding transferred electron numbers and H_2O_2 production (b and c), and the Tafel plots of each electrodes (d).

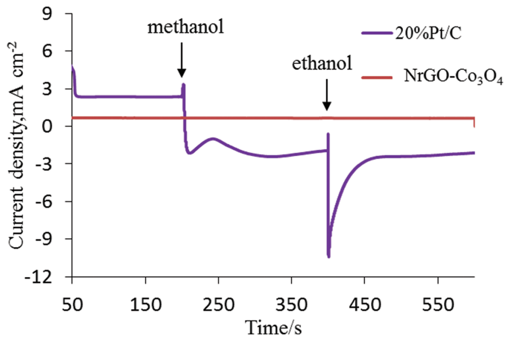

Figure 8. Chronoamperometric response of NrGO–Co_3O_4 and Pt/C with addition of 1 M methanol and ethanol, respectively.

transfer inside NrGO–Co_3O_4, which is better than NrGO and similar to Pt/C. The results indicate that the similar behaviors of the Tafel slopes and the reaction mechanism and the rate-determining step is much better at NrGO–Co_3O_4 catalyst.[36,44]

3.3. Crossover Effect

The crossover effect is also a critical issue in FCs application. To investigate the crossover effect of the NrGO–Co_3O_4 electrocatalysts toward ORR, we performed amperometric measurement on NrGO–Co_3O_4 and 20% Pt/C electrodes at -0.3 V (vs. Ag/AgCl) in an O_2 saturated 0.1 M KOH electrolyte (Fig. 8). As shown in Figure 8, a sharp signal change in current is observed at Pt/C electrode upon addition of 1 M methanol and ethanol, respectively. However, the corresponding amperometric response for the NrGO–Co_3O_4 modified electrode remains nearly unchanged after the addition of methanol and ethanol. This result strongly indicates that the NrGO–Co_3O_4 electrocatalyst has higher fuel selectivity toward ORR than that of commercial Pt/C electrocatalyst.

4. CONCLUSIONS

A simple method is reported for the synthesis of NrGO–Co_3O_4 and NrGO electrocatalysts which have been demonstrated as catalysts for ORR. The structural, morphological properties and stability have been deduced from TEM, XPS and Raman spectra analysis. The ORR activity was evaluated by RDE technique in O_2 saturated alkaline medium. K–L plot proved that the hydrogen peroxide by product formation using NrGO–Co_3O_4 was lesser than NrGO, and it followed four electron transfer pathway mechanism. Kinetic parameter such as Tafel slope (120 mV dec^{-1}) is indicating one electron transfer as rate determining step. The kinetic current density, E_{onset} and half wave potential values confirm that NrGO–Co_3O_4 has better ORR activity than NrGO. The as synthesized NrGO–Co_3O_4 electrocatalysts showed better alcohol-like fuel tolerance than commercial Pt/C (20 wt%).

Acknowledgments: This research has supported by the National Research Foundation of Korea (NRF) funded by the Ministry of Education, Science and Technology (NRF-2015R1D1A1A09059344).

References and Notes

1. R. Bashyam and P. Zelenay, *Nature* 443, 63 (**2006**).
2. M. S. Ahmed and S. Jeon, *ACS Catal.* 4, 1830 (**2014**).
3. H. S. Han, M. S. Ahmed, H. Jeong, and S. Jeon, *J. Nanosci. Nanotechnol.* 16, 333 (**2016**).
4. J. E. Choe, J.-M. You, M. Yun, K. Lee, M. S. Ahmed, Z. Üstündag, and S. Jeon, *J. Nanosci. Nanotechnol.* 15, 5684 (**2015**).
5. H. Jeong, M. S. Ahmed, and S. Jeon, *J. Nanosci. Nanotechnol.* 11, 987 (**2011**).
6. G. Wu, K. L. More, C. M. Johnston, and P. Zelenay, *Science* 332, 443 (**2011**).
7. M. S. Ahmed and S. Jeon, *J. Power Sources* 218, 168 (**2012**).
8. M. Yun, M. S. Ahmed, and S. Jeon, *J. Power Sources* 293, 380 (**2015**).
9. J. E. Choe, M. S. Ahmed, and S Jeon, *J. Electrochem. Soc.* 163, B113 (**2016**).
10. Y. J. Wang, D. P. Wilkinson, and J. J. Zhang, *Chem. Rev.* 111, 7625 (**2011**).
11. A. Serov and C. Kwak, *Appl. Catal. B Environ.* 90, 313 (**2009**).
12. X. Lin, Y. Liu, S. D. Poynton, A. L. Ong, J. R. Varcoe, L. Wu, Y. Li, X. Liang, Q. Li, and T. Xu, *J. Power Sources* 233, 259 (**2013**).
13. M. S. Ahmed, H. Jeong, J.-M. You, and S. Jeon, *Electrochim. Acta* 56, 4924 (**2011**).
14. H. Yun, M. S. Ahmed, K. Lee, S. Jeon, C. W. Lee, *Appl. Surf. Sci.* 360, 915 (**2016**).
15. K. Geim and K. S. Novoselov, *Nat. Mater.* 6, 183 (**2007**).
16. S. Yasmin, M. S. Ahmed, and S. Jeon, *J. Electrochem. Soc.* 162, B363 (**2015**).
17. A. Ejaz, M. S. Ahmed, and S. Jeon, *Sens. Actuators B* 221, 1256 (**2015**).
18. M. D. Stoller, S. J. Park, Y. W. Zhu, J. H. An, and R. S. Ruoff, *Nano Lett.* 8, 3498 (**2008**).
19. F. Zhang, T. Zhang, X. Yang, L. Zhang, K. Leng, Y. Huang, and Y. Chen, *Energy Environ. Sci.* 6, 1623 (**2013**).
20. L. F. Lai, *Energy Environ. Sci.* 5, 7936 (**2012**).
21. L. Y. Feng, *Sci. Rep.* 3, 3306 (**2013**).
22. Y. Xu, X. Wang, C. An, Y. Wang, L. Jiao, and H. Yuan, *J. Power Sources* 272, 328 (**2014**).
23. G. D. Park, J. S. Cho, and Y. C. Kang, *Nano Energy* 17, 17 (**2015**).
24. M. S. Ahmed, D. Park, and S. Jeon, *J. Power Sources* 308, 180 (**2016**).
25. Y. Liang, Y. Li, H. Wang, J. Zhou, J. Wang, T. Regier, and H. Dai, *Nat. Mater.* 10, 780 (**2011**).
26. M. S. Ahmed, J.-M. You, H. S. Han, D.-C. Jeong, and S. Jeon, *J. Nanosci. Nanotechnol.* 14, 5722 (**2014**).
27. J. E. Choe, M. S. Ahmed, and S. Jeon, *J. Electrochem. Soc.* 163, B113 (**2016**).
28. H. Begum, M. S. Ahmed, and S. Jeon, *RSC Adv.* 6, 50572 (**2016**).
29. M. S. Ahmed and S. Jeon, *J. Nanosci. Nanotechnol.* 13, 306 (**2013**).
30. M. S. Ahmed, D. Kim, and S. Jeon, *Electrochim. Acta* 92, 168 (**2013**).
31. M. S. Ahmed and S. Jeon, *J. Power Sources* 282, 479 (**2015**).
32. Y. Zhang, J. Ge, L. Wang, D. Wang, F. Ding, X. Tao, and W. Chen, *Sci. Rep.* 3, 2771 (**2013**).
33. J. Pu, Z. Wang, K. Wu, N. Yu, and E. Sheng, *Phys. Chem. Chem. Phys.* 16, 785 (**2014**).
34. A. C. Mtukula, J. Shen, X. Bo, and L. Guo, *J. Alloys Compounds* 655, 229 (**2016**).
35. K. Lee, M. S. Ahmed, and S. Jeon, *J. Power Sources* 288, 261 (**2015**).

36. M. S. Ahmed, H. S. Han, and S. Jeon, *Carbon* 61, 164 **(2013)**.
37. M. Li, X. Bo, Y. Zhang, C. Han, A. Nsabimana, and L. Guo, *J. Mater. Chem. A* 2, 1167 **(2014)**.
38. W. Chen and S. Chen, *Angew. Chem. Int. Ed.* 48, 4386 **(2009)**.
39. D. Kim, M. S. Ahmed, and S. Jeon, *J. Mater. Chem.* 22, 16353 **(2012)**.
40. S. M. S. Kumar, J. S. Herrero, S. Irusta, and K. Scott, *J. Electroanal. Chem.* 647, 211 **(2010)**.
41. J. Zhu, M. Xiao, C. Liu, J. Ge, J. S. Pierre, and W. Xing, *J. Mater. Chem. A* 3, 21451 **(2015)**.
42. L. Demarconnay, C. Coutanceau, and J.-M. Leger, *Electrochim. Acta* 49, 4513 **(2004)**.
43. S. J. Amirfakhri, D. Binny, J.-L. Meunier, and D. Berk, *J. Power Sources* 257, 356 **(2014)**.
44. J. E. Choe, M. S. Ahmed, and S. Jeon, *J. Power Sources* 281, 211 **(2015)**.
45. M. S. Ahmed and S. Jeon, *J. Electrochem. Soc.* 161, F1300 **(2014)**.
46. M. S. Ahmed, D. Kim, H. S. Han, H. Jeong, and S. Jeon, *J. Nanosci. Nanotechnol.* 12, 8349 **(2012)**.
47. R. Liu, Y. Jin, P. Xu, X. Xing, Y. Yang, and D. Wuc, *J. Colloid Interface Sci.* 464, 83 **(2016)**.
48. Y. Wang, X. Ma, L. Lu, Y. He, X. Qi, and Y. Deng, *Int. J. Hydrogen Energy* 38, 13611 **(2013)**.
49. M. Zhang, R. Li, X. Chang, C. Xue, and X. Gou, *J. Power Sources* 290, 25 **(2015)**.
50. Y. Liu, J. Li, W. Li, Y. Li, Q. Chen, and F. Zhan, *J. Power Sources* 299, 492 **(2015)**.

Received: 22 March 2016. Accepted: 23 May 2016.